Journal of
Materials Chemistry C

PAPER

View Article Online
View Journal

Cite this: DOI: 10.1039/c5tc03464g

7,7′-Diazaisoindigo: a novel building block for organic electronics†

Gustavo de Miguel,[a] Luis Camacho[a] and Eva M. García-Frutos*[b]

Received 22nd October 2015,
Accepted 4th January 2016

DOI: 10.1039/c5tc03464g

www.rsc.org/MaterialsC

In this paper, a new family of 7,7′-diazaisoindigo molecules was synthesized and the electronic properties of these materials were studied by theoretical calculations and photophysical studies. Density functional theory (DFT) calculations at the B3LYP/6-311+G** level of theory demonstrate that the diaza-substitution clearly imposes a higher planarity in these molecules compared to the isoindigo counterparts. This effect is ascribed to an electrostatic attraction between the carbonyl group and the H atom at position 4. The isodensity surfaces and energies of the frontier molecular orbitals (HOMO and LUMO) calculated at the B3LYP/6-311++G(2d,p) level of theory show a stabilization (~0.35 eV) of both orbitals in the 7,7′-diazaisoindigo derivatives compared to isoindigo and also the intramolecular charge-transfer character for the HOMO → LUMO transition, as it occurs in isoindigo. Photophysical studies were carried out using steady-state and time-resolved picosecond fluorescence techniques. The emission spectra show a red-shift of the peak upon increasing the polarity of the solvents which confirms the charge-transfer character of this transition. Moreover, the intensity of the emission peak decreases with the solvent polarity and increases in viscous solvents, which is tentatively attributed to a non-radiative deactivation pathway connected with a torsion of the central ethylene bond. The time-resolved emission technique shows shorter fluorescence lifetimes with increasing polarity of the solvents, in line with the stronger quenching of the fluorescence signal. The appearance of fluorescence peaks and relatively long fluorescence lifetimes in the 7,7′-diazaisoindigo derivatives compared to the non-fluorescent isoindigo counterpart are ascribed to the fine adjustment of the orbital energies through the aza insertion in the isoindigo core structure. This is a consequence of the slower non-radiative process in 7,7′-diazaisoindigo which may help to promote the use of this building block instead of isoindigo in organic electronics.

1. Introduction

Organic π-conjugated molecules play special and key roles in magnetism, conductance, and photonics due to the π-electronic communication. In particular, small π-conjugated organic molecules have many advantages because of their unique optical and electronic properties. Thus, their tunable properties are based on the synthesis and ability to modify the size and the shape of the organic structure. Over the past few decades, research on organic molecules has been growing rapidly because of their promising application in organic electronics,[1,2] such as organic photovoltaics (OPVs),[3–6] organic light-emitting devices (OLEDs),[7,8] and organic field-effect transistors (OFETs).[9–11]

Different classes of small π-conjugated organic materials (donor and acceptor moieties), conductors and semiconductors have attracted much attention in recent times. However, organic compound acceptors with a high reactivity and stability remain less described. Different acceptor families, such as naphthalene diimides (NDIs),[12–14] perylene imides (PDIs),[15] diketopyrrolopyrrole (DPP)[16] and bithiophene imides (BTIs),[17] based on amide/imide have been described. Among all these acceptors the amide/imide based materials present an excellent ambient stability. One of the most recent amide/imide acceptors employed to date for the organic electronics are isoindigo molecules.[18] Isoindigo has been extensively investigated as an electron deficient building block for organic electronic[18–23] but there exist relatively little works on the modification of its core. One variation of the isoindigo core structure is 7-azaisoindigo which has been investigated for its use in medicinal chemistry, although only one work describes its use in optoelectronic applications.[24]

[a] Institute of Fine Chemistry and Nanochemistry, Department of Physical Chemistry and Applied Thermodynamics, University of Córdoba, Campus Universitario de Rabanales, Edificio Marie Curie, Córdoba, E-14014, Spain
[b] Instituto de Ciencia de Materiales de Madrid (ICMM), CSIC, Cantoblanco, Madrid, E-28049, Spain. E-mail: emgfrutos@icmm.csic.es; Fax: +34 91 372 0623; Tel: +34 91 334 9038

† Electronic supplementary information (ESI) available: Experimental details, theoretical calculations, electrochemical measurements, absorption and emission studies, and ^{1}H NMR and ^{13}C NMR spectral data. See DOI: 10.1039/c5tc03464g

In an effort to prepare new small π-conjugated organic materials based on isoindigo derivatives for their future optoelectronic applications, in this paper we report the synthesis of new 7,7′-diazaisoindigo derivatives. Theoretical calculations with density functional theory (DFT) and photophysical investigations by using steady-state and time-resolved picosecond fluorescence techniques were performed to characterize the electronic properties of these materials. A rational comparison with the properties of the isoindigo counterpart is realized, highlighting the main advantages of these novel building blocks in the field of molecular electronics.

2. Experimental

2.1. Materials and methods

All starting materials were acquired from commercial suppliers. Oxygen gas sensitive reaction was performed under an atmosphere of nitrogen. Column chromatography was carried out on silica gel (200–300 meshes). NMR spectra were obtained using a Bruker AVANCE 200 MHz spectrometer. Chemical shifts (δ) are quoted in parts per million (ppm), referenced to residual solvent. All the theoretical calculations were performed using the Spartan 14 software. The molecular geometries of the different compounds in the gas phase were optimized without symmetry constraints by density functional theory (DFT) using the B3LYP hybrid functional and the 6-311+G** basis set. The single energy point calculations were all computed at the B3LYP/6-311++G(2d,p) level of theory and the vertical transition energies of **2c** and *N*,*N*-dibutyl isoindigo were calculated using time-dependent DFT (TD-DFT) at the B3LYP/6-311++G(2d,p) level of theory. The electrochemical measurements were performed on a CHI650A electrochemical workstation from IJ Cambria.

UV-visible absorption spectra were measured on a Cary 100 Bio UV-visible spectrophotometer. Steady-state and time-resolved fluorescence measurements were performed on a FLS920 Fluorimeter (Edinburgh Instrument Ltd, Livingston, UK).

3. Results and discussion

3.1. Synthesis of compounds 2a–c

The synthesis of **2** derivatives is shown in Scheme 1. The commercially available 7-azaindole served as a starting material for the preparation of 7-azaindolin-2-one and 7-azaisatin which has been previously described.[25,26] The synthesis of 7-azaindolin-2-one was prepared in 79% overall yield by treatment with pyridinium perbromide followed by debromination[25] and 7-azaisatin by the oxidation of 7-azaindolin-2-one using NBS/DMSO.[27]

The final condensation between 7-azaindolin-2-one and 7-azaisatin in the presence of *p*-toluenesulfonic acid (PTSA)[28] affords 7,7′-diazaisoindigo in 93% yield. The synthesis of the *N*,*N*-dialkyl derivatives (**2a–c**, Scheme 1) was achieved by the alkylation of **1** with different alkyl iodide derivatives in the presence of K_2CO_3 as the base in dimethylformamide (DMF), providing **2a–c** in moderate yields. The presence of long alkyl chains on the nitrogen functionalities of **2** confers to this molecule enhanced solubility and lowers its melting point. Moreover, the alkyl chains facilitate the processability of this material while the electronic properties and geometry of the platform are not affected.

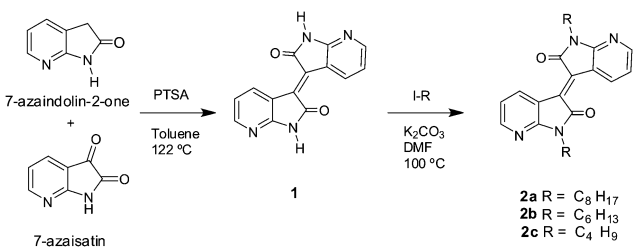

Scheme 1 Synthesis of compounds **2**.

3.2. Theoretical calculations

Density functional theory (DFT) calculations were utilized to determine the optimized geometries and frontier orbital energy levels for **2a–c** and *N*,*N*-dibutyl isoindigo. The latter molecule is used as a reference in the following discussion due to the evident structural similarities with the 7,7′-diazaisoindigo derivatives and the existence of good theoretical calculations of the ground and excited state of the parent molecule: isoindigo.

Fig. 1A depicts the optimized molecular geometry for **2c** and *N*,*N*-dibutyl isoindigo calculated at the B3LYP/6-311+G** level of theory. Interestingly, the minimized structures differ in the value of the dihedral angle (twisting angle between the two aza-oxindole moieties), with 4° and 16° for **2c** and *N*,*N*-dibutyl

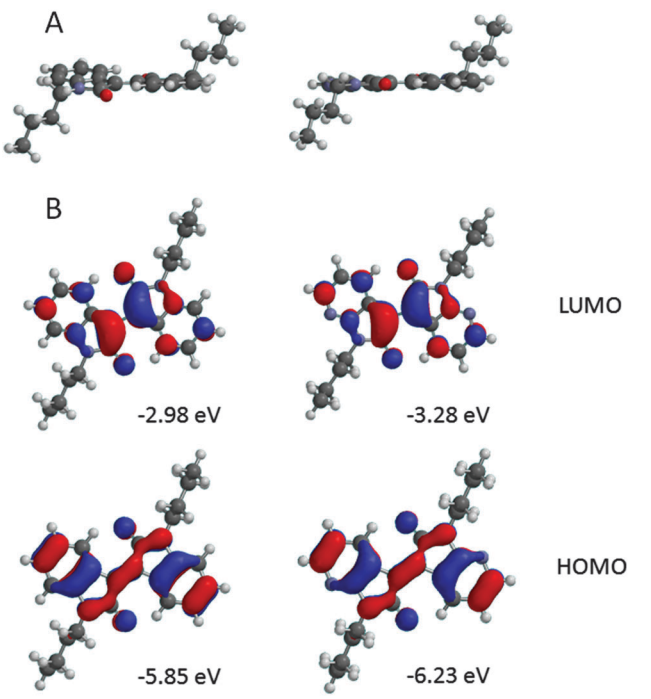

Fig. 1 (A) Optimized molecular geometries for *N*,*N*-dibutyl isoindigo (left) and **2c** (right) calculated at the B3LYP/6-311+G** level of theory. (B) Frontier molecular orbitals and energies of *N*,*N*-dibutyl isoindigo (left) and **2c** (right) calculated at the B3LYP/6-311++G(2d,p) level of theory.

isoindigo, respectively. The latter value for the isoindigo derivative is in line with that observed in the literature for the unsubstituted and *N*,*N*-dimethyl isoindigo, ~15°, which reflects the poor influence of the *N*-alkyl chain on the twisting angle (no steric hindrance).[29,30] In the diazaisoindigo compounds, the same behavior was observed, a negligible change in the twisting angle in the compounds with longer *N*-alkyl chains, 3° and 4° for **2a** and **2b**, respectively (see Fig. S1, ESI†). Thus, the diaza-substitution in **2a–c** clearly imposes a higher planarity in the molecule, which constitutes a relevant result due to the small change with respect to the isoindigo counterpart. The dihedral angle in this family of compounds is basically governed by the planarization effect of the π-conjugated backbone and the steric hindrance constraining the system to some rotation around the central double bond. However, the insertion of the N atom should not affect significantly the previous two factors. We tend to ascribe the change in the dihedral angle to electrostatic attractions between the carbonyl groups and the H atoms bound to the C at position 4 of each aza-oxindole moiety. Thus, the higher electronegativity of N *vs.* C atoms results in a partial positive charge on the C atoms in the pyridine-like moiety due to mesomeric and inductive effects. This behavior can be visualized using electrostatic potential maps, which describes the interaction energy of the molecules with a positive point charge (see Fig. S2, ESI†). Thus, a more positive potential in **2c** compared to *N*,*N*-dibutyl isoindigo is observed at the H atom attached to the C atom in position 4. We believe that this extra positive charge in **2c** generates an electrostatic attraction with the partial negative charge of the carbonyl group favoring the planarization of the molecule.

Fig. 1B illustrates the isodensity surfaces (0.032 e $bohr^{-3}$) and energies of the frontier molecular orbitals of **2c** and *N*,*N*-dibutyl isoindigo calculated at the B3LYP/6-311++G(2d,p) level of theory. The same surfaces were calculated for **2a** and **2b** (see Fig. S3, ESI†). The aza-substitution leads to some variation of the frontier orbital energies (FOEs): both the HOMO and the LUMO are stabilized by a similar energy, ~0.35 eV. This effect is entirely attributed to the electron donating character of the N atom in the aza-oxindole moieties since similar results have been reported in pyridine-like structures with no significant change in the energy gap between the HOMO and the LUMO.[31] A close examination of the LCAO coefficients of the HOMO and the LUMO reveals that the location of these orbitals is nearly identical in both molecules. The HOMO is homogeneously distributed in the π-conjugated region (stilbene unit) while the LUMO is preferably localized at the oxo-pyrrolidine moieties. This configuration denotes a certain intramolecular charge-transfer character for the HOMO → LUMO transition, as it has been previously indicated for isoindigo.[29] In the 7,7′-diaza-isoindigo derivatives, the stronger electron-donating character of the pyridine group may reinforce the charge transfer nature of the lowest-energy transition. Finally, the dipole moments for the ground states were calculated. Interestingly, the 7,7′-diaza-isoindigo molecules possess an almost zero ground state dipole moment (~0.02 D) in opposition to the value obtained for *N*,*N*-dibutylisoindigo (0.6 D), which coincides well with that reported for *N*,*N*-dimethyl isoindigo (~0.5 D). This result is explained because of the different dihedral angles in the two molecules.

TD-DFT calculations were also performed at the B3LYP/6-311++G(2d,p) level of theory to investigate the vertical excited state transitions. **2c** presents two vertical transitions centered at 3.85 and 2.59 eV with oscillator strengths of 0.51 and 0.16, respectively. The low-energy transition is mainly HOMO → LUMO (89%), while in the high-energy one the HOMO−2 → LUMO is prevailing (70%). In the case of *N*,*N*-dibutyl isoindigo, there are three main vertical transitions at 3.48, 3.18 and 2.47 eV with oscillator strengths of 0.54, 0.12 and 0.10, respectively. While the lowest energy transition is clearly a HOMO → LUMO (85%) as for **2c**, the other two are mixed configurations with one-electron transitions from HOMO−2 → LUMO and HOMO−3 → LUMO. The results for *N*,*N*-dibutyl isoindigo match nicely with those reported for the *N*,*N*-dimethyl isoindigo.[29]

3.3. Electrochemical measurements

With the aim of understanding the redox behavior of the 7,7′-diazaisoindigo compounds, cyclic and differential pulse voltammetry experiments were realized for the three derivatives. Fig. S4 (ESI†) shows the cyclic and differential pulse voltammograms of compound **2c** in CH_2Cl_2 using $TBAPF_6$ as the supporting electrode. Both techniques feature two reversible reduction peaks at −1.21 and −1.62 V with respect to the Fc/Fc^+ couple. The same reduction potentials were observed for **2a** and **2b**. This behaviour is consistent with the electron accepting character of the isoindigo derivatives. Compared to the *N*,*N*′-dihexylisoindigo counterpart (E_{red} = −1.4 and −1.8 V),[29] the 7,7′-diazaisoindigo compounds present easier one and two electron reductions. This result corroborates the lower energy of the LUMO in **2** with respect to the *N*,*N*-dibutyl isoindigo obtained in the theoretical calculations, which was ascribed to the insertion of the N atom in the isoindigo structure.

3.4. Photophysical studies

A. Steady-state absorption and emission. The 7,7′-diaza-isoindigo compounds synthesized in this article belong to the family of indigo compounds, which present a rich photophysical activity characterized by the strong absorption in the UV-visible region. In particular, our compounds are closely related to isoindigo, but the phenyl rings included in each oxindole moiety were replaced by pyridine groups. In the following, the photophysics of the 7,7′-diazaisoindigo compounds is studied in different solvents by using steady-state and time-resolved spectroscopy techniques and a rational comparison with the behavior of isoindigo is carried out.

Fig. 2A shows the normalized (at λ = 284 nm) UV-vis absorption spectra of the three studied molecules in CCl_4 (5×10^{-5} M). The spectra resemble clearly the same as those for the three molecules – also in solvents with increasing polarity CH_2Cl_2, EtOH and ACN – which demonstrate that the length of the side alkyl chains does not influence the absorption properties of the π-conjugated system. Three absorption bands

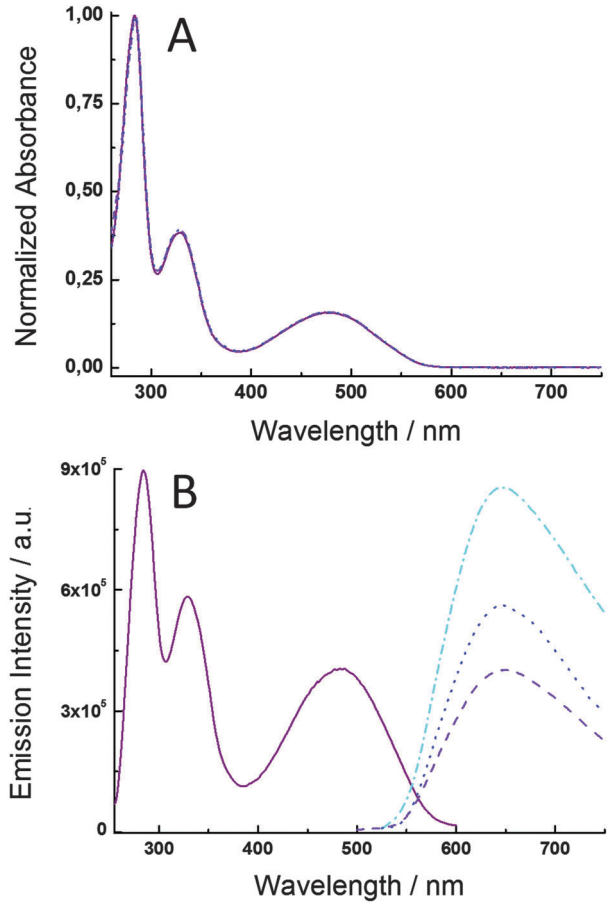

Fig. 2 (A) Normalized (at λ = 284 nm) absorption spectra of the three investigated molecules, **2c** (purple solid line), **2b** (violet dashed line) and **2a** (blue dotted line) in CCl_4. (B) Excitation (purple solid line, λ_{em} = 650 nm) and emission spectra of **2b** in CCl_4 at different excitation wavelengths, λ_{exc} = 475 nm (violet dashed line), λ_{exc} = 330 nm (blue dotted line) and λ_{exc} = 280 nm (light blue dotted-dashed line).

centered at λ_{max} = 284, 329 and 477 nm are observed in the spectra, with the latter one wider than the other two. Isoindigo also presents three absorption peaks at similar positions, but with the second peak being more shifted to longer wavelengths, $\lambda \sim$ 395 nm.[32] The extinction coefficients (ε) for the absorption peaks in CCl_4 are ε = 2700, 6700 and 17600 L mol^{-1} cm^{-1} at the λ_{max} value from the low to the high energy peaks, which are comparable to those measured for isoindigo.[32] The TD-DFT calculations predicted well the position and strength of the two low-energy absorption peaks (λ_{max}^{theor} = 322 and 479 nm), with the broad red-shifted band exhibiting charge transfer character, and the central band being assigned to local electronic transitions.[29] On the other hand, absorption spectra of the three molecules in different solvents were also measured. Fig. S5 (ESI†) displays almost no change in the shape and maxima of the absorption peaks in solvents with increasing polarity: CCl_4 (ε = 2.24), toluene (ε = 2.38), CH_2Cl_2 (ε = 8.93), cyclohexanol (ε = 15.0), EtOH (ε = 24.5) and ACN (ε = 37.5). Only a 4 nm blue shift of the low-energy peak in EtOH and ACN was found which matches perfectly with the almost zero value of the dipole moment for the ground state in these molecules. This behavior is comparable to that of isoindigo and derivatives, although a slightly more intense shift is observed in the absorption spectra due to the larger value of the dipole moment (0.5–0.6 D).[29,33]

Fig. 2B shows the emission spectra of **2b** in CCl_4 under excitation at the maxima of the three absorption peaks, λ_{exc} = 280, 330 and 475 nm. The shape of the emission band remains the same independent of the excitation wavelength and is centered at λ_{max} = 645 nm. The same behavior (λ_{max} and shape) was observed for the other two molecules with shorter and longer *N*-alkyl chains, **2a** and **2c**, which again suggests the reduced influence of the side chains in the photophysics of the molecules. Interestingly, in opposition to the evident emission band in our molecules, the well-studied counterpart – isoindigo – does not fluoresce at all.[29,33] Nevertheless, the fluorescence quantum yield is rather low (Φ_{fluor} = 0.003 for **2b** in CCl_4), which reveals that this radiative process is not the principal deactivation mechanism of the excited state. Recently, 6,6′-isoindigo derivatives have been reported to present weak emission peaks at around 675 nm in toluene ($\Phi_{fluor} < 0.001$).[29] The latter peaks are very broad which confirms that both emission signals (from **2** and 6,6′-isoindigo) may develop from similar excited states sharing similar deactivation channels. Fig. 2B also shows the excitation spectrum of **2b** at λ_{em} = 650 nm, with three peaks matching perfectly those observed in the absorption spectrum. The latter indicates that the higher excited states (S_2 and S_3) associated with the two high-energy absorption peaks (λ_{abs} = 284 and 329 nm) are deactivated *via* internal conversion to the charge transfer state (S_1). However, the relative intensity of the peaks in the excitation spectrum is different from that found in the absorption spectrum, with lower intensity for the two high-energy peaks. This behavior points out that the quantum yield for internal conversion is not 100% and the higher excited states are partially deactivated through other mechanisms.

To investigate the deactivation mechanism of the first singlet excited state (S_1), the emission spectra were also measured in solvents with increasing polarity. Fig. 3a displays the spectra of **2b** in seven solvents upon excitation at the maximum of the low-energy band, λ_{exc} = 475 nm. Noticeably, there is a good correlation between the intensity of the signal and the polarity of the solvent, the higher the dielectric constant of the solvent is the lower will be the emission peak. The same relationship was also found with the other two molecules, **2a** and **2c** (Fig. S6, ESI†). However, one of the used solvents presented a higher viscosity with respect to the others, cyclohexanol (η = 57.5 cP). The emission spectrum in this solvent did not follow the good correlation with respect to the solvent polarity. Indeed, the intensity of the emission spectrum of **2b** in cyclohexanol is higher than that in anisole, despite the fact that the dielectric constant is ~4 times smaller for the latter solvent (ε = 15.0 *vs.* 4.33). This behavior suggests the presence of a deactivation pathway (non-radiative process) that is influenced by high viscosity solvents. The molecular structure of these compounds, and their counterpart isoindigo, resembles to that of *trans*-stilbene, which is a model system (together with ethylene) in the study of *cis–trans* photoisomerization. The relaxation dynamics of

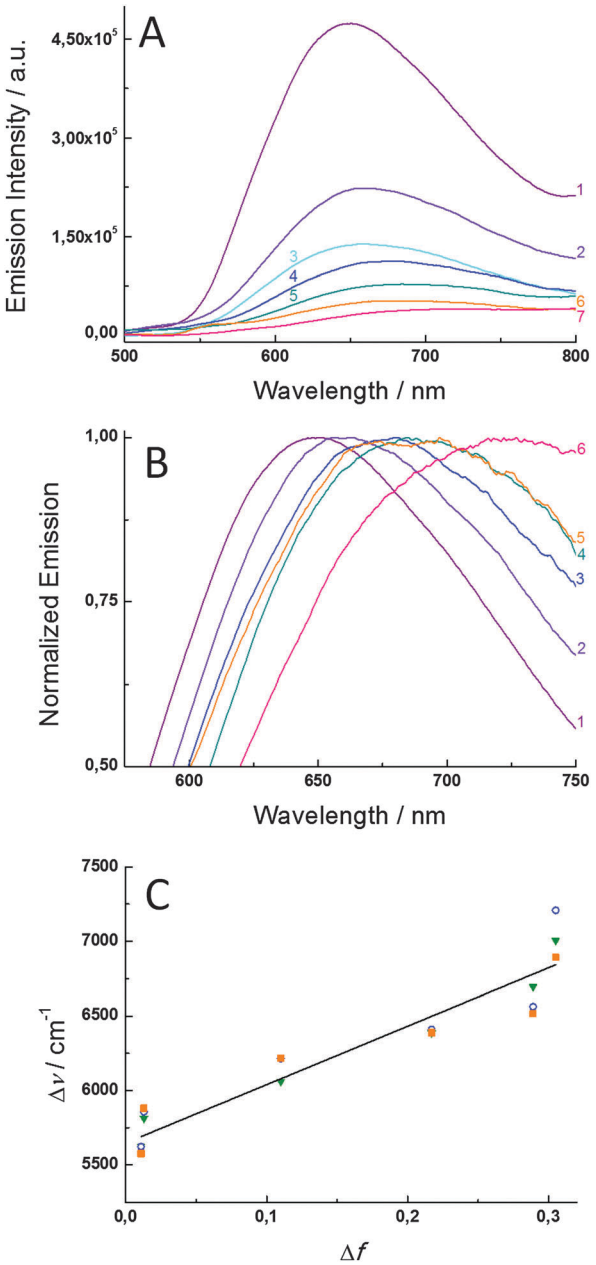

Fig. 3 (A) Emission spectra of **2b** in different solvents: CCl_4 (1), toluene (2), cyclohexanol (3), anisole (4), CH_2Cl_2 (5), EtOH (6) and ACN (7). λ_{exc} = 475 nm. (B) Normalized emission spectra of **2b** in different solvents: CCl_4 (1), toluene (2), anisole (3), CH_2Cl_2 (4), EtOH (5) and ACN (6). λ_{exc} = 475 nm. (C) Stokes shift $\Delta\nu$ *versus* Δf for the three investigated molecules, **2a** (green triangles), **2b** (blue circles) and **2c** (orange squares). The straight line is the best linear fit to the data points of **2a**.

trans-stilbene could provide some indications explaining the fluorescence quenching in the 7,7′-diazaisoindigo derivatives. In particular, the main deactivation pathway of the excited state in *trans*-stilbene is a non-radiative process *via* a conical intersection (CI) which involves a twisting of the double bond followed by pyramidalization of one of the ethylenic carbon atoms.[34] Thus, the enhancement of the fluorescence signal of **2** in cyclohexanol could be explained since the high viscosity slows down the bond rearrangement (non-radiative deactivation). Moreover, the strong quenching of the fluorescence signal upon increasing the solvent polarity can be ascribed to the existence of intramolecular electron transfer processes linked to the rearrangement of the bonds. The energy barrier required to achieve the CI is decreased at higher polarizability of the solvents, accelerating this non-radiative process.

In addition to the decrease of the intensity with the solvent polarity, the emission spectra show a shift of the wavelength of the maximum absorption (λ_{max}). Fig. 3b shows the normalized emission spectra of **2b** illustrating the solvent-dependent spectral shifts of this molecule. It is worth noting that the shape of the spectra remains the same for all the solvents, which rules out the appearance of a new spectral component. A close inspection of the spectra displays a red-shift of the λ_{max} at growing polarity, from λ_{max} = 650 to λ_{max} = 719 nm, when going from toluene to ACN. The same tendency is observed in the other two molecules, **2a** and **2c** (see Fig. S7, ESI†). The Lippert–Mataga equation was used to account for general interactions between the fluorophore and the solvent, plotting the Stokes shift ($\Delta\nu$) *vs.* the orientation polarizability (Δf), which is a factor including the changes in the refractive index and the dielectric constant of the solvents. Fig. 3c shows a good linear relationship of these two parameters (correlation coefficient, r = 0.94 for **2b**). Moreover, the slope of the fit ($3.9 \pm 0.8 \times 10^3$ cm^{-1} for **2b**) is relatively high which indicates a strong change of the dipole moment upon excitation. Thus, assuming the radius of the cavity, a = 4 Å, which is reasonable for considering the dimensions of the molecules, it is possible to calculate the dipole moment of the excited state, $\mu_e \approx 5.0$ D. Indeed, the theoretical calculations already showed the intramolecular charge-transfer character of the first excited state (S_1), which explains the large value of the dipole moment in the excited state.

B. Time-resolved picosecond fluorescence. To shed much light on the photophysics of the three molecules, the kinetics of the different deactivation pathways were studied by time-resolved picosecond emission spectroscopy. Table 1 shows the fluorescence lifetimes (τ) obtained from monoexponential fits of the emission signal for the three molecules in seven different solvents.

There is a good correlation between the lifetimes and the orientation polarizability parameter (Δf). For example, in **2b**,

Table 1 Fluorescence lifetimes derived from a monoexponential fit of the experimental data for the three studied molecules in seven different solvents. λ_{exc} = 440 nm. The parameters of the solvent are also given (dielectric constant ε, Lippert–Mataga solvent polarity parameter Δf, and viscosity η at 293 K)

	2a	**2b**	**2c**	Solvent properties		
Solvent	τ/ps	τ/ps	τ/ps	ε	Δf	η/cp
CCl_4	105	117	114	2.24	0.011	0.91
Toluene	70	86	84	2.38	0.013	0.56
Anisole	63	59	56	4.33	0.110	1.05
CH_2Cl_2	<40	<40	<40	8.93	0.217	0.41
Cyclohexanol	53	52	54	15	0.230	57.5
EtOH	<40	<40	<40	24.5	0.289	1.07
ACN	<40	<40	<40	37.5	0.305	0.37

Table 2 Photophysical properties of **2b** in seven different solvents. T = 298 K

Solvent	$\Phi_{fl} \times 10^4$	τ/ps	$k_{fl} \times 10^{-7}$ s^{-1}	$k_{IC} \times 10^{-10}$ s^{-1}
CCl_4	28	117	2.4	0.8
Toluene	14	86	1.6	1.2
Anisole	6.6	59	1.1	1.7
CH_2Cl_2	4.6	<40	>1.1	>2.5
Cyclohexanol	8.4	52	1.3	1.9
EtOH	3.1	<40	>0.8	>2.5
ACN	2.3	<40	>0.6	>2.5

τ decreases from 117 to 86 and 59 ps, in CCl_4, toluene and anisole, respectively. In the more polar solvents, CH_2Cl_2, EtOH and ACN, the lifetimes are much shorter (<40 ps), below the detection limit of the instrument. Moreover, in cyclohexanol, τ is similar to that in anisole (*e.g.* 54 *vs.* 56 ps for **2c**), despite the double value of Δf. This is again ascribed to the much higher viscosity of cyclohexanol (η = 57.5 *vs.* 1.05 cp in anisole), which is hypothesized to slow down the twisting of the double bond after excitation. With all these arguments in mind, we believe that there are two main mechanisms of deactivation of the excited state (S_1): radiative deactivation through fluorescence emission and internal conversion *via* a rearrangement of the bonds possibly through a twisting of the double bond. The possibility of intersystem crossing has been explored by carrying out singlet oxygen experiments, but no phosphorescence emission at 1270 nm was detected. Thus, the kinetics rate constants for both deactivation pathways (k_{fl} and k_{IC}), determined by using classical eqn (1) and (2), are shown in Table 2.

$$k_{fl} = \frac{\Phi_{fl}}{\tau_{S_1}} \quad (1)$$

$$k_{IC} = \frac{1}{\tau_{S_1}} - k_{fl} \quad (2)$$

Firstly, the values of k_{fl} are very similar for the different solvents, which confirms that the solvent properties do not affect the radiative deactivation. Secondly, there is a clear increase of the k_{fl} value upon increasing the polarity of the solvent that can be explained due to a decrease of the activation energy since the polar solvents stabilize the charge-transfer twisted state. In stilbene, the bond rearrangement causes a photoisomerization of the molecule, which eventually ends up in the more stable *trans* photoisomer. Moreover, similar indole-based molecules with ability to rotate through a central double bond were reported to suffer photoisomerization and the back kinetics was probed using transient absorption techniques.[35] Thus, flash-photolysis measurements were performed for the three 7,7′-diazaisoindigo molecules to investigate the formation of long-lived species, in particular, the photoisomers. However, no signal at all was detected in the nano- to millisecond time regime, which indicates that the twisted state must deactivate rapidly to the ground state through the possible conical intersection.

Next, a particular analysis is performed to compare the emission lifetimes in the 7,7-diazaisoindigo molecules with those observed in isoindigo and derivatives. The absence of fluorescence emission in isoindigo was tentatively ascribed to a particularly fast non-radiative deactivation pathway due to analogy with *trans*-stilbene (τ_{fl} = 79 ps in hexane).[29] In our molecules, the existence of fluorescence with relatively long lifetimes is a key factor that differentiates it from isoindigo. From a structural point of view, since the extension of the *N*-alkyl chains does not alter the lifetimes, the aza groups must exert a notable influence on the non-radiative process, assuming a similar rate constant for the radiative process. A recent report has claimed a lowering of the LUMO energy in 7-azaisoindigo based chromophores, which might indicate an increase of the activation energy of the twisting processes.[24] The latter would result in a decrease of the non-radiative process and therefore longer fluorescence lifetimes. Moreover, 6,6′-isoindigo derivatives were recently found to exhibit fluorescence emission in opposition to 5,5′-derivatives. This result further emphasizes the importance of substitution in isoindigo, where small structural changes can have a deep impact on the photophysics. Thus, we tend to attribute the detection of fluorescence (with long lifetimes) in the 7,7′-diaza-isoindigo molecules to a reduced rate constant for the non-radiative process compared to that in isoindigo.

Finally, the deceleration of the non-radiative process in 7,7′-diazaisoindigo is relevant for the applications of the isoindigo-family of chromophores. For example, in dye-sensitized solar cells, the quantum yield of the electron injection reaction is strongly dependent on the kinetics of the non-radiative processes since the electron injection (picosecond time scale) competes with the other deactivation mechanism. Thus, utilization of less flexible units has been proposed in indoline-based dyes to preclude the twisting of ethylene groups (non-radiative deactivation).[36] We have proved a longer fluorescence lifetime in the 7,7′-diaza-isoindigo derivatives by fine adjustment of the orbital energies through the aza insertion in the isoindigo core structure. Thereby, the slower non-radiative process in **2** is expected to facilitate the electron separation reactions in organic solar cells compared to isoindigo-based devices.

4. Conclusions

In summary, we have prepared different alkyl chain 7,7′-diaza-isoindigo derivatives. The presence of the long alkyl chains on the nitrogen functionalities confers to the molecule enhanced solubility, and facilitates the processability of this material while the electronic properties and geometry of the platform are not affected. DFT studies have demonstrated a quasi-planar structure in the 7,7′-diazaisoindigo derivatives due to an electrostatic interaction between the carbonyl groups and H atoms in position 4. Both the HOMO and the LUMO are stabilized ($\sim$0.35 eV) compared to the isoindigo counterpart and the HOMO → LUMO transition presents an intramolecular charge-transfer character as in isoindigo. The photophysical studies have proved fluorescence quenching and shorter lifetimes in solvents with increasing polarity and opposite behavior in solvents with higher viscosity. These results are ascribed to the presence of a non-radiative deactivation pathway *via* a conical intersection (CI) as it occurs in the similar molecule, stilbene.

More theoretical calculations are planned to shed much light on the rearrangement of the molecule conducting to the CI. Finally, the fine adjustment of the orbital energies through the aza insertion in the isoindigo core structure implies a slower non-radiative process in 7,7′-diazaisoindigo. As a consequence of this, relatively long fluorescence lifetime is found in the 7,7′-diazaisoindigo derivatives compared to isoindigo (no fluorescence). The longer lifetime of the S_1 state involves an advantage for molecular electronics which may help to stimulate the use of this building block instead of isoindigo. For example, the electron injection efficiency in dye-sensitized solar cells is expected to be improved from long-lived excited states.

Acknowledgements

This work was financially supported by the MICINN of Spain (CTQ2013-40562-R). G. M. thanks the Ministry of Economy and Competitiveness for a ''Ramón y Cajal'' contract (RYC-2013-12772). G. M. and L. C. acknowledge the Ministry of Economy and Competitiveness for financial support (CTQ2014-56422-P). The authors want to thank R. Estévez for his help with the electrochemical measurements.

Notes and references

1 E. M. Garcia-Frutos, *J. Mater. Chem. C*, 2013, **1**, 3633–3645.
2 S. Ogawa, *Organic Electronics Materials and Devices*, Springer, 2015.
3 A. W. Hains, Z. Liang, M. A. Woodhouse and B. A. Gregg, *Chem. Rev.*, 2010, **110**, 6689–6735.
4 K. A. Mazzio and C. K. Luscombe, *Chem. Soc. Rev.*, 2015, **44**, 78–90.
5 Y. Liu, J. Zhao, Z. Li, C. Mu, W. Ma, H. Hu, K. Jiang, H. Lin, H. Ade and H. Yan, *Nat. Commun.*, 2014, **5**, 5293.
6 G. Yu, J. Gao, J. C. Hummelen, F. Wudl and A. J. Heeger, *Science*, 1995, **270**, 1789–1791.
7 C. Zhong, C. Duan, F. Huang, H. Wu and Y. Cao, *Chem. Mater.*, 2011, **23**, 326–340.
8 J.-H. Jou, S. Kumar, A. Agrawal, T.-H. Li and S. Sahoo, *J. Mater. Chem. C*, 2015, **3**, 2974–3002.
9 J. Zaumseil and H. Sirringhaus, *Chem. Rev.*, 2007, **107**, 1296–1323.
10 C. Wang, H. Dong, W. Hu, Y. Liu and D. Zhu, *Chem. Rev.*, 2012, **112**, 2208–2267.
11 C. Zhang, P. Chen and W. Hu, *Chem. Soc. Rev.*, 2015, **44**, 2087–2107.
12 J. Choi, K.-H. Kim, H. Yu, C. Lee, H. Kang, I. Song, Y. Kim, J. H. Oh and B. J. Kim, *Chem. Mater.*, 2015, **27**, 5230–5237.
13 H. U. Kim, J.-H. Kim, H. Kang, A. C. Grimsdale, B. J. Kim, S. C. Yoon and D.-H. Hwang, *ACS Appl. Mater. Interfaces*, 2014, **6**, 20776–20785.
14 M. Sommer, *J. Mater. Chem. C*, 2014, **2**, 3088–3098.
15 C. Li and H. Wonneberger, *Adv. Mater.*, 2012, **24**, 613–636.
16 A. D. Hendsbee, J.-P. Sun, L. R. Rutledge, I. G. Hill and G. C. Welch, *J. Mater. Chem. A*, 2014, **2**, 4198–4207.
17 N. Zhou, X. Guo, R. P. Ortiz, S. Li, S. Zhang, R. P. H. Chang, A. Facchetti and T. J. Marks, *Adv. Mater.*, 2012, **24**, 2242–2248.
18 R. Stalder, J. Mei, K. R. Graham, L. A. Estrada and J. R. Reynolds, *Chem. Mater.*, 2014, **26**, 664–678.
19 T. Lei, J.-Y. Wang and J. Pei, *Acc. Chem. Res.*, 2014, **47**, 1117–1126.
20 K. Mahmood, Z.-P. Liu, C. Li, Z. Lu, T. Fang, X. Liu, J. Zhou, T. Lei, J. Pei and Z. Bo, *Polym. Chem.*, 2013, **4**, 3563–3574.
21 T. Lei, Y. Cao, Y. Fan, C.-J. Liu, S.-C. Yuan and J. Pei, *J. Am. Chem. Soc.*, 2011, **133**, 6099–6101.
22 J. Mei, K. R. Graham, R. Stalder and J. R. Reynolds, *Org. Lett.*, 2010, **12**, 660–663.
23 A. Yassin, P. Leriche, M. Allain and J. Roncali, *New J. Chem.*, 2013, **37**, 502–507.
24 N. M. Randell, A. F. Douglas and T. L. Kelly, *J. Mater. Chem. A*, 2014, **2**, 1085–1092.
25 A. Marfat and M. P. Carta, *Tetrahedron Lett.*, 1987, **28**, 4027–4030.
26 R. Sriram, C. N. Sesha Sai Pavan Kumar, N. Raghunandan, V. Ramesh, M. Sarangapani and V. J. Rao, *Synth. Commun.*, 2012, **42**, 3419–3428.
27 X. Cheng, K.-H. Merz, S. Vatter, J. Christ, S. Wölfl and G. Eisenbrand, *Bioorg. Med. Chem.*, 2014, **22**, 247–255.
28 F. Bouchikhi, F. Anizon and P. Moreau, *Eur. J. Med. Chem.*, 2008, **43**, 755–762.
29 L. A. Estrada, R. Stalder, K. A. Abboud, C. Risko, J.-L. Brédas and J. R. Reynolds, *Macromolecules*, 2013, **46**, 8832–8844.
30 E. A. Perpète, J. Preat, J.-M. André and D. Jacquemin, *J. Phys. Chem. A*, 2006, **110**, 5629–5635.
31 D. Chen, S.-J. Su and Y. Cao, *J. Mater. Chem. C*, 2014, **2**, 9565–9578.
32 P. W. Sadler, *Spectrochim. Acta*, 1960, **16**, 1094–1099.
33 S. Luňák Jr, P. Horáková and A. Lyčka, *Dyes Pigm.*, 2010, **85**, 171–176.
34 J. Quenneville and T. J. Martínez, *J. Phys. Chem. A*, 2003, **107**, 829–837.
35 G. de Miguel, M. Marchena, M. Zitnan, S. S. Pandey, S. Hayase and A. Douhal, *Phys. Chem. Chem. Phys.*, 2012, **14**, 1796–1805.
36 A. M. El-Zohry, D. Roca-Sanjuán and B. Zietz, *J. Phys. Chem. C*, 2015, **119**, 2249–2259.